



Mesoscopic Constructs of Ordered and Oriented Metal–Organic Frameworks on Plasmonic Silver Nanocrystals

Yingbo Zhao,^{†,‡} Nikolay Kornienko,^{†,‡} Zheng Liu,[‡] Chenhui Zhu,[§] Shunsuke Asahina,[⊥] Tsung-Rong Kuo,[†] Wei Bao,[†] Chenlu Xie,[†] Alexander Hexemer,[§] Osamu Terasaki,^{||,∇} Peidong Yang,^{*,†} and Omar M. Yaghi^{*,†,¶}

[†]Department of Chemistry, University of California—Berkeley, Materials Sciences Division, Lawrence Berkeley National Laboratory, and Kavli Energy NanoSciences Institute, Berkeley, California 94720, United States

[‡]Nanotube Research Center, National Institute of Advanced Industrial Science and Technology (AIST), Tsukuba 305-8565, Japan

[§]Advanced Light Source, Lawrence Berkeley National Laboratory, Berkeley, California 94720, United States

[⊥]SMBU, JEOL Ltd., Akishima, Tokyo 196-8558, Japan

^{||}Department of Materials and Environmental Chemistry and EXSELENT, Stockholm University, SE-106 91 Stockholm, Sweden

[∇]Graduate School of EEWS, WCU/BK21Plus, Korea Advanced Institute of Science and Technology (KAIST), Daejeon 305-701, Republic of Korea

[¶]King Abdulaziz City of Science and Technology, P.O. Box 6086, Riyadh 11442, Saudi Arabia

S Supporting Information

ABSTRACT: We enclose octahedral silver nanocrystals (Ag NCs) in metal–organic frameworks (MOFs) to make mesoscopic constructs O_h -nano-AgCMOF in which the interface between the Ag and the MOF is pristine and the MOF is ordered (crystalline) and oriented on the Ag NCs. This is achieved by atomic layer deposition of aluminum oxide on Ag NCs and addition of a tetra-topic porphyrin-based linker, 4,4',4'',4'''-(porphyrin-5,10,15,20-tetrayl)-tetrabenzoic acid (H_4 TCPP), to react with alumina and make MOF $[Al_2(OH)_2TCPP]$ enclosures around Ag NCs. Alumina thickness is precisely controlled from 0.1 to 3 nm, thus allowing control of the MOF thickness from 10 to 50 nm. Electron microscopy and grazing angle X-ray diffraction confirm the order and orientation of the MOF by virtue of the porphyrin units being perpendicular to the planes of the Ag. We use surface-enhanced Raman spectroscopy to directly track the metalation process on the porphyrin and map the distribution of the metalated and unmetalated linkers on a single-nanoparticle level.

Inorganic nanocrystals (NCs) are important because they occupy a size regime intermediate between small molecules and extended structures. Their chemistry has been largely explored through surface functionalization. The fundamental problem is that it is difficult to control the spatial arrangement and order of the functional units and, thus, the chemistry occurring at the interface between the inorganic NC and an incoming substrate. We believe that this “functionalization problem” could be overcome by using metal–organic frameworks (MOFs) as well-defined units for which the spatial arrangement of functional organic and inorganic units, porosity, density, and thickness can be precisely controlled. Addressing this problem requires a new synthetic approach to overcome four challenges: a pristine interface between inorganic NCs and

MOFs that is free of surfactants and other surface ligands to take advantage of synergistic effects at the interface; well-ordered and precisely oriented MOF enclosures around the inorganic NCs to impart a high degree of spatial control over the desired functional groups; sufficiently thin MOF enclosures for facile diffusion and high-resolution chemical mapping; and bridging multiple length scales by combining the MOF's atomically defined scale with the nano dimension for plasmonic structures, thus realizing new chemical and physical functions. In this way, it would be possible to construct mesoscopic assemblies where the MOF and the plasmonic NCs are linked across multiple length scales yet operate differently and synergistically.

Although efforts to grow MOFs on inorganic NCs have been made, a general method addressing all four challenges has not emerged.¹ In this work, a general method is developed to overcome these four challenges using atomic layer deposition (ALD), where a thin metal oxide film is deposited onto plasmonic Ag NCs and used as a metal ion source to nucleate the desired MOF when the appropriate organic linker is added. We show that ALD allows control of MOF thickness by controlling the metal oxide thickness, while the slow release of metal ions from the metal oxide layer controls the crystallinity of the MOF and ultimately its orientation on the Ag NCs. The MOF's crystallinity and orientation, and the pristine interface thus produced, enable metalation and linker variation chemistry to be carried out on the MOF–Ag NC mesoscopic construct. Integration of MOFs on NC surfaces further enables the direct probing of such chemistry by surface-enhanced Raman spectroscopy (SERS) using the plasmonic Ag NC substrates. Specifically, we show that the course of metalation in a porphyrin-based MOF can be tracked, and different chemical signatures within MOFs can be imaged at high spatial resolution down to the single-nanoparticle (NP) level.

Received: December 19, 2014

Published: January 26, 2015



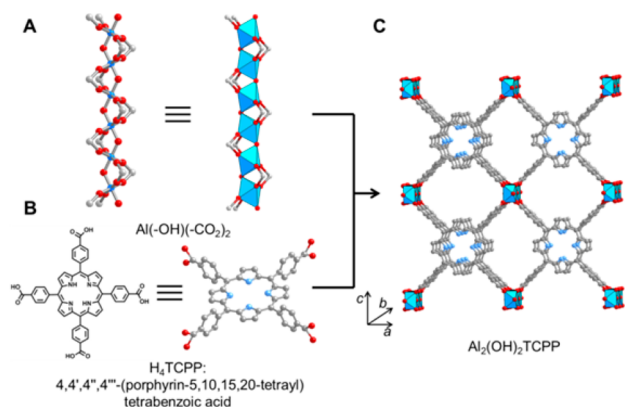


Figure 1. Structure of $\text{Al}_2(\text{OH})_2\text{TCPP}$ MOF. Construction of $\text{Al}_2(\text{OH})_2\text{TCPP}$ MOF from (A) rod-shaped aluminum oxide units linked by (B) porphyrin units (H_4TCPP) to give a three-dimensional MOF (C) having $0.11 \times 0.60 \text{ nm}^2$ opening along the b -axis. Al, blue octahedra and blue spheres in (A); N, blue spheres; O, red spheres; C, gray spheres. H atoms are omitted for clarity.

Our strategy involves making Ag NP–MOF constructs (O_h -nano-AgCMOF) in which Ag NPs are wrapped by MOF enclosures. Ag octahedra were synthesized by the polyol method: silver nitrate salt is reduced by a pentanediol solvent and polyvinylpyrrolidone (PVP) used as surfactant.² Ag NCs are selected as a model plasmonic metal nanostructure as they have intense local surface plasmon resonances in the visible range and have been extensively studied as SERS substrates.³ The chosen MOF is $\text{Al}_2(\text{OH})_2\text{TCPP}$ [$\text{H}_4\text{TCPP} = 4,4',4'',4'''$ -(porphyrin-5,10,15,20-tetrayl)tetrabenzoic acid], which consists of chains of corner-sharing Al octahedra running along the b -axis and connected by the TCPP units through the carboxylate groups (Figure 1).⁴ This MOF was synthesized in bulk by reacting H_4TCPP with AlCl_3 in water at 180°C to give a large-microcrystalline powder.

With the eventual goal of creating thin films of this MOF on the Ag surface, we chose to use ALD thin films as a localized metal precursor source. Fabrication of the O_h -nano-AgCMOF begins with deposition of Al_2O_3 films on the Ag NCs as the Al source for the MOF synthesis. The Ag NC is drop-cast on a silicon substrate, and conformal, thickness-controlled alumina is deposited at 60°C using trimethylaluminum and water as precursors at a deposition rate of 0.1 nm/cycle (Supporting Information (SI), Figure S1). The alumina-coated Ag NCs are converted to a MOF by reacting with the TCPP linker. However, the original hydrothermal condition used to synthesize this MOF would not be appropriate, as the high temperature will melt the Ag NCs and the TCPP linker is not soluble enough in water to sufficiently react with alumina. Considering this, the reaction temperature was reduced to 140°C , and N,N -dimethylformamide (DMF)/water mixed solvent is used, containing 5 mg of H_4TCPP dissolved in 1.5 mL of DMF and 0.5 mL of H_2O . The conversion of alumina to MOF was carried out in a sealed glass tube in a microwave reactor using initially 20 nm thick layers of alumina. Unfortunately, an interfacial 10 nm thick alumina layer between the MOF and the Ag was observed instead of the desired pristine interface. This led us to reduce the alumina layer thickness to $<3 \text{ nm}$, which we found to be sufficient to eliminate the interfacial alumina layer while enabling the fabrication of conformal and thin MOF enclosures.

We next used Raman spectroscopy to characterize the MOF composition of the thin film and detect the signature of the

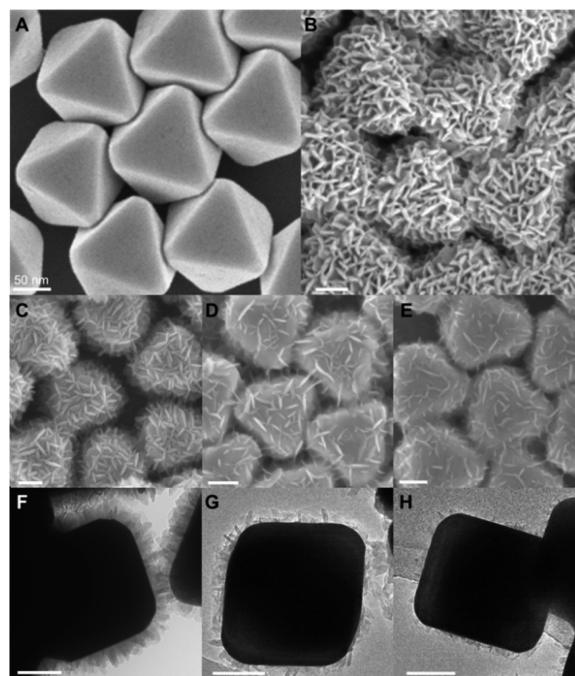


Figure 2. SEM and TEM images of the O_h -nano-AgCMOF particles. Octahedral Ag NCs (A) are subjected to ALD deposition of alumina, followed by addition of TCPP linkers to make MOF-enclosed Ag NCs, O_h -nano-AgCMOF (B). Variation in the alumina thickness from 3 to 0.5 to 0.1 nm allows control of MOF coverage on the Ag NCs, with their SEM (C–E) and TEM (F–H) images further confirming the thickness and coverage of the MOF. The black square-like figure in F–H is the Ag NC. Scale bars = 50 nm .

porphyrin building units in the MOF, but we found that the PVP at the interface between Ag and MOF gave a strong signal that overwhelmed the Raman spectrum. We addressed this issue by using an additional surface cleaning step using a Meerwein's salt treatment to remove PVP surfactant before coating the Ag with ALD alumina to ensure a pristine interface between the MOF and Ag NC (Figure S2).⁵ Following surfactant removal, the MOF conversion was carried out again, and only the strong TCPP signal was visible in the Raman spectrum (Figure S3).

Grazing incidence wide-angle X-ray scattering (GIWAXS) measurements confirmed the phase purity and high crystallinity of the MOF enclosures synthesized using 1, 5, and 30 cycles of ALD Al_2O_3 (Figure S4). Scanning electron microscopy (SEM), used to characterize the morphology of O_h -nano-AgCMOF, showed that the shape of the Ag NC is retained throughout the fabrication process and crystalline plate-like MOF regions are visible on the Ag NC surface (Figures 2A,B and S5).

We proceeded to quantify the thickness control of the resulting MOF enclosures by controlling the ALD layer thickness. Figure 2 shows typical SEM and transmission electron microscopy (TEM) images of MOF films obtained from alumina layer thicknesses of 3 , 0.5 , and 0.1 nm (Figure 2C–H). With increased cycles of alumina, the size and coverage of MOF crystallites on the Ag surface as well as the overall MOF layer thickness increase. The average thickness of the MOF enclosures is ~ 50 , 25 , and 10 nm for 30 cycles, 5 cycles, and 1 cycle of alumina ALD, respectively (Figure 2F–H). At the lowest limits of the ALD precursor film thickness of $<1 \text{ nm}$, highly crystalline MOF enclosures as thin as several nanometers are made (Figure S6). The crystallite size and morphology of the MOF are finely tuned by varying the reaction conditions: a 3:1 water/DMF

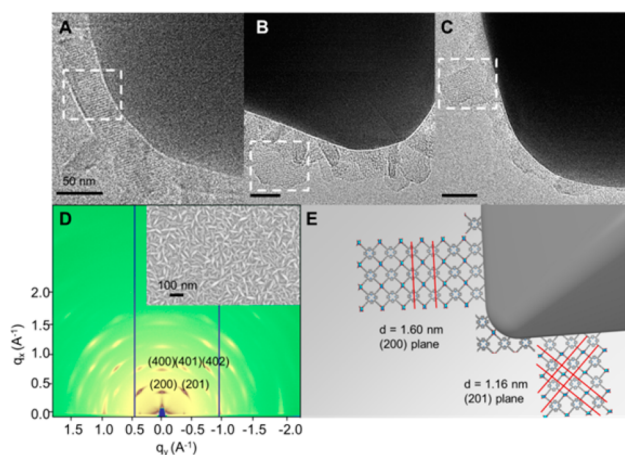


Figure 3. Order (crystallinity) and orientation of MOFs on the Ag NC interface. High-resolution TEM of O_h -nano-AgCMOF shows MOF lattice fringes of 1.16 nm (bordered by dotted rectangle) (A), corresponding to the MOF (201) planes, which clearly shows a pristine interface with the Ag NCs (large darkened shapes). MOF orientation is confirmed by the lattice fringes of 1.60 nm (bordered by dotted rectangle) (B), corresponding to the MOF (200) planes and indicating that the porphyrin units in the MOF enclosure are perpendicular to the Ag NC surface. Lattice fringes of 1.16 nm (bordered by dotted rectangle) (C) further confirm this orientation, in this case recorded along two directions, corresponding to the (201) planes. The crystallinity of the MOF enclosure and its orientation in O_h -nano-AgCMOF are confirmed by the GIWAXS diffraction plot (D), which shows a spot pattern indicative of high crystallinity and preferred orientation. The in-plane diffraction spots of MOF (200) and (400) planes indicate the porphyrin units are perpendicular to the substrates, with the b -axis parallel to the substrate (D,E).

solvent mixture results in a more uniform, conformal MOF enclosure in contrast to the plate-like structure (Figure S7).

The MOF crystallinity and orientation at the interface were examined by high-resolution TEM. Imaging under the accelerating voltage of 120 kV with a low electron dosage showed MOF lattice fringes (Figure 3A). This confirms, at a microscopic level, the high crystallinity of the MOF enclosure at the interface and the fact that it is pristine. The orientation of the MOF regions was determined from the TEM images (Figure 3B), where the lattice fringes of 1.60 nm correspond to the MOF (200) planes parallel to the interface. This indicates that the porphyrin units of the MOF are perpendicular to the Ag surface. Two-dimensional lattice fringes of 1.16 nm, corresponding to MOF (201) planes, are also observed (Figure 3C), providing unambiguous determination that the MOF is perpendicular to the Ag surface. Detailed analysis of the Ag and MOF orientation is described in the SI (section S3). No evidence of porphyrin units oriented parallel to the Ag surface was found in the TEM images. Energy-dispersive X-ray spectroscopy (EDS) elemental mapping was used to further confirm the enclosed structure of the O_h -nano-AgCMOF, as described further below.

GIWAXS structural analysis is performed on a macroscopic level using a flat silicon substrate for MOF growth to further confirm the crystallinity and orientation of the MOF at an ensemble level. The spot pattern on the GIWAXS image (Figure 3D) matches that expected for the preferred orientation of the MOF with the porphyrin units perpendicular to the substrate (MOF [200] direction perpendicular to the substrate). A random orientation of the MOF would result in a ring rather than a spot pattern in the GIWAXS image. This oriented growth

is also observed when glass is used as the substrate to grow the MOF (Figure S16), which suggests that the oriented MOF growth is not substrate specific. The TEM and GIWAXS findings combined lead to a structural model of the MOF–substrate interface (Figure 3E) in which the porphyrin units of the MOF are perpendicular to the interface. This clearly demonstrates that this synthetic approach is well-suited for fabricating crystalline and precisely oriented MOF enclosures on inorganic NCs. Knowledge of the porphyrin orientation relative to the Ag NCs also conveys their spatial arrangement and allows us to carry out, for the first time on a NC substrate, chemistry specific to the porphyrin units (metalation with cobalt, see below) and probe it by SERS. We note that these constructs can be made on other substrates such as carbon disk and other MOFs (SI, section S4, and Figures S22–S27).

In an O_h -nano-AgCMOF sample, all peaks in the SERS spectrum match those of the bulk MOF and the TCPP molecule and can be assigned according to previous literature studies of porphyrin molecules (Figure S3).⁶ This spectroscopic handle allowed us to track the metalation of the porphyrin units within the MOF enclosure. Metalation was carried out by heating the O_h -nano-AgCMOF in a 10 mg/mL cobalt acetate/methanol solution at 100 °C under microwave irradiation (SI, section S6). Metalation of the porphyrin molecule is evidenced mainly by the decline of the ν_8 mode, corresponding to the free base porphyrin at 330 cm^{-1} , and the rise of the ν_8 mode of the metalated porphyrin at 390 cm^{-1} .^{6a} This is further confirmed by UV–vis (Figure S28) and EDS, where in the latter elemental mapping is used to further confirm the enclosed structure of the O_h -nano-AgCMOF (Figure S29). Within the enclosure of MOF, this post-synthetic metalation is tracked with SERS (Figure 4A) and found to be complete within 50 min.

Confocal SERS mapping is next applied to study heterogeneous MOF enclosures on Ag NCs and the unique ability of this system to generate spatially resolved chemical information. The size of an O_h -nano-AgCMOF octahedron is 300 nm, similar to the diffraction-limited spatial resolution possible with a 532 nm laser in a confocal microscopy setup. Thus, chemical information at the limit of a single Ag NP can be obtained. The multivariate approach, in which different organic linkers are incorporated into the same framework, is a powerful technique to introduce heterogeneity and complexity into MOFs and has presented challenges to its characterization due to a lack of techniques capable of deciphering the spatial arrangement of the linkers.⁷

The premetalated porphyrin linker, cobalt(II) 4,4',4'',4'''-(porphyrin-5,10,15,20-tetrayl)tetrabenzic acid, was mixed with the unmetalated TCPP linker in a 1:3 ratio in the precursor solution and reacted with the alumina-coated Ag NCs under the conditions described above. The SERS spectrum was measured on clusters of O_h -nano-AgCMOF particles and found to have peaks attributable to the ν_8 mode of both metalated and unmetalated forms of the porphyrin unit (Figure 4B). A fundamental difficulty in nano-MOF chemistry is to decipher whether the NPs as a whole are homogeneous in their composition, especially when a multivariate approach is used. The materials prepared here allow us to address this issue. Mapping of the metalated and unmetalated linkers in a monolayer of O_h -nano-AgCMOF (Figure S40) using SERS reveals a well-mixed porphyrin system, in which, on the single-particle level, there is no segregation of metalated and unmetalated regions of the MOF (Figure 4C,D). This is quantified by the ratio of the Raman scattering intensity of the two ν_8 modes for the metalated and unmetalated regions. This

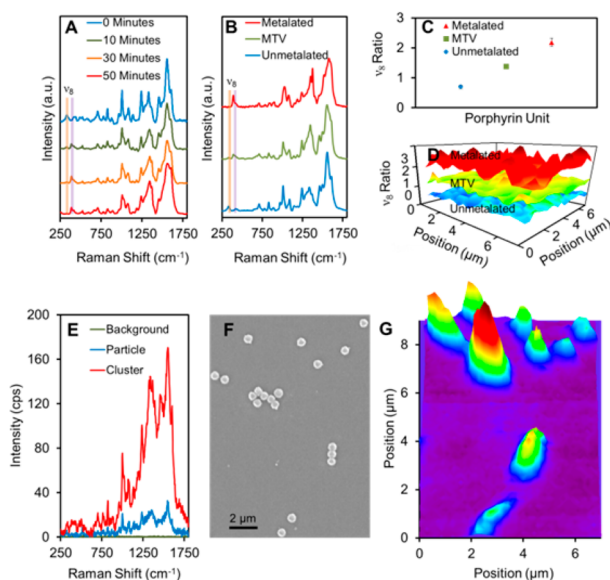


Figure 4. Tracking metalation of MOF linkers and mapping of metalated and unmetalated linkers in O_h -nano-AgCMOF using SERS. Time-dependent SERS spectroscopic tracking of metalation of the porphyrin linker units (A) showing the evolution of the ν_8 mode and the completion of reaction within 50 min. The SERS spectra for metalated, unmetalated, and multivariate metalated O_h -nano-AgCMOF (B) show that the system is multivariate. The ratio of metalated and unmetalated linkers (C) and the homogeneity of these in the O_h -nano-AgCMOF particles packed into a monolayer (Figure S40) (D) are mapped (color going from blue to red corresponding to the value of the ν_8 mode ratio going from 0.5 to 3.5). SERS enhancement is shown for single particles and clusters of O_h -nano-AgCMOF (E), along with SEM of spatially resolved discrete O_h -nano-AgCMOF (F) and the result of their SERS mapping (G), showing the 1:1 correspondence.

ratio is obtained by integrating the corresponding peak areas and is found to lie at 1.5, which is in between all metalated and all unmetalated scenarios (Figure 4C), indicating that the distribution is homogeneous from particle to particle, as evidenced from mapping 7 μm regions (Figure 4D and SI, section S8).

To illustrate the power of combining MOFs and plasmonic NCs into one mesoscopic construct, O_h -nano-AgCMOF, we examined an area occupied by multiple discrete particles for their chemical composition using confocal Raman spectroscopy. It is very clear that, because of the thin enclosure of MOF around the Ag, it is possible to observe strong SERS signals for each of the particles, and furthermore, within each such particle, the metalated and unmetalated porphyrin units in the MOF can be observed. Figure 4F,G shows the area of particles and their corresponding SERS maps. Comparison of them also reveals that the SEM and SERS mappings are consistent in providing a highly resolved picture of the spatial arrangement of the mesoscopic O_h -nano-AgCMOF particles.

■ ASSOCIATED CONTENT

● Supporting Information

Details of synthesis and characterization. This material is available free of charge via the Internet at <http://pubs.acs.org>.

■ AUTHOR INFORMATION

Corresponding Authors

*p_yang@berkeley.edu

*yaghi@berkeley.edu

Author Contributions

#Y.Z. and N.K. contributed equally.

Notes

The authors declare no competing financial interest.

■ ACKNOWLEDGMENTS

This research was partially supported by BASF SE (Ludwigshafen, Germany) for bulk synthesis of MOF, and Director, Office of Science, Office of Basic Energy Sciences, Materials Sciences and Engineering Division, U.S. Department of Energy, under Contract No. DE-AC02-05CH11231 for plasmonic nanocrystals. We acknowledge Mr. J. Resasco and Dr. S. Brittman for help with the ALD, and Dr. K. Bustillo, Dr. H. Furukawa, and Dr. Y. Zhang for helpful discussion. This work made use of facilities at the Molecular Foundry and the National Center of Electron Microscopy at Lawrence Berkeley National Laboratory (LBNL), at the Nanotube Research Center, National Institute of Advanced Industrial Science and Technology (AIST), and at SMBU, JEOL, Tokyo. Work at the Molecular Foundry is supported by the Office of Science, Office of Basic Energy Sciences, U.S. Department of Energy, under Contract No. DE-AC02-05CH11231. GIWAXS measurements were performed at the Advanced Light Source (ALS) at LBNL. The ALS is an Office of Science User Facility operated for the U.S. Department of Energy Office of Science by LBNL and supported by the U.S. Department of Energy under Contract No. DE-AC02-05CH11231. Y.Z. is supported by the Suzhou Industrial Park fellowship. Z.L. acknowledges Grant-in-Aid for Scientific Research (C) (25390023).

■ REFERENCES

- (1) (a) He, L.; Liu, Y.; Liu, J.; Xiong, Y.; Zheng, J.; Liu, Y.; Tang, Z. *Angew. Chem., Int. Ed.* **2013**, *52*, 3741–3745. (b) Hu, P.; Zhuang, J.; Chou, L.-Y.; Lee, H. K.; Ling, X. Y.; Chuang, Y.-C.; Tsung, C.-K. *J. Am. Chem. Soc.* **2014**, *136*, 10561–10564. (c) Hu, Y.; Liao, J.; Wang, D.; Li, G. *Anal. Chem.* **2014**, *86*, 3955–3963. (d) Jin, S.; Son, H.-J.; Farha, O. K.; Wiederrecht, G. P.; Hupp, J. T. *J. Am. Chem. Soc.* **2013**, *135*, 955–958. (e) Khaletskaya, K.; et al. *J. Am. Chem. Soc.* **2013**, *135*, 10998–11005. (f) Kreno, L. E.; Greeneltch, N. G.; Farha, O. K.; Hupp, J. T.; Van Duyne, R. P. *Analyst* **2014**, *139*, 4073–4080. (g) Kreno, L. E.; Hupp, J. T.; Van Duyne, R. P. *Anal. Chem.* **2010**, *82*, 8042–8046. (h) Liu, N.; Yao, Y.; Cha, J.; McDowell, M.; Han, Y.; Cui, Y. *Nano Res.* **2012**, *5*, 109–116. (i) Lu, G.; et al. *Nat. Chem.* **2012**, *4*, 310–316. (j) Reboul, J.; et al. *Nat. Mater.* **2012**, *11*, 717–723. (k) Shekhah, O.; Wang, H.; Strunskus, T.; Cyganik, P.; Zacher, D.; Fischer, R.; Wöll, C. *Langmuir* **2007**, *23*, 7440–7442. (l) So, M. C.; Jin, S.; Son, H.-J.; Wiederrecht, G. P.; Farha, O. K.; Hupp, J. T. *J. Am. Chem. Soc.* **2013**, *135*, 15698–15701. (m) Sugikawa, K.; Furukawa, Y.; Sada, K. *Chem. Mater.* **2011**, *23*, 3132–3134. (n) Zhan, W.-w.; Kuang, Q.; Zhou, J.-z.; Kong, X.-j.; Xie, Z.-x.; Zheng, L.-s. *J. Am. Chem. Soc.* **2013**, *135*, 1926–1933.
- (2) Tao, A.; Sinsermsuksakul, P.; Yang, P. *Angew. Chem., Int. Ed.* **2006**, *45*, 4597–4601.
- (3) (a) Tao, A.; Sinsermsuksakul, P.; Yang, P. *Nat. Nanotechnol.* **2007**, *2*, 435–440. (b) Tao, A. R.; Ceperley, D. P.; Sinsermsuksakul, P.; Neureuther, A. R.; Yang, P. *Nano Lett.* **2008**, *8*, 4033–4038.
- (4) Fateeva, A.; Chater, P. A.; Ireland, C. P.; Tahir, A. A.; Khimiyak, Y. Z.; Wiper, P. V.; Darwent, J. R.; Rosseinsky, M. J. *Angew. Chem., Int. Ed.* **2012**, *51*, 7440–7444.
- (5) Rosen, E. L.; Buonsanti, R.; Llordes, A.; Sawvel, A. M.; Milliron, D. J.; Helms, B. A. *Angew. Chem., Int. Ed.* **2012**, *51*, 684–689.
- (6) (a) Vlckova, B.; Matejka, P.; Simonova, J.; Cermakova, K.; Pancoska, P.; Baumruk, V. *J. Phys. Chem.* **1993**, *97*, 9719–9729. (b) Li, X. Y.; Czernuszewicz, R. S.; Kincaid, J. R.; Su, Y. O.; Spiro, T. G. *J. Phys. Chem.* **1990**, *94*, 31–47.
- (7) Kong, X.; Deng, H.; Yan, F.; Kim, J.; Swisher, J. A.; Smit, B.; Yaghi, O. M.; Reimer, J. A. *Science* **2013**, *341*, 882–885.